COO-1198-1137

THE RECOVERY OF LEAD AFTER ELECTRON IRRADIATION AT 1.5 K

Robert Charles Birtcher

Department of Physics and Materials Research Laboratory

University of Illinois, Urbana, Illinois 61801

May 1975

This technical information document is based on a thesis submitted in partial fulfillment of the requirements for the degree of Doctor of Philosophy in Physics in the Graduate College of the University of Illinois, 1975. This research was supported in part by the U. S. Atomic Energy Commission under Contract AT(11-1)-1198.

DISCLAIMER

C00-1198-1137

THE RECOVERY OF LEAD AFTER ELECTRON IRRADIATION AT 1.5 K

Robert Charles Birtcher

Department of Physics and Materials Research Laboratory

University of Illinois, Urbana, Illinois 61801

May 1975

This technical information document is based on a thesis submitted in partial fulfillment of the requirements for the degree of Doctor of Philosophy in Physics in the Graduate College of the University of Illinois, 1975. This research was supported in part by the U. S. Atomic Energy Commission under Contract AT(11-1)-1198.

THE RECOVERY OF LEAD AFTER ELECTRON IRRADIATION AT 1.5 K

Robert Charles Birtcher, Ph.D
Department of Physics
University of Illinois at Urbana-Champaign, 1975

The low temperature recovery of lead following an electron irradiation at 1.5 K shows the same features observed for all face-centered-cubic metals except for gold. The Stage I occurs below 5.5 K. The I_D recovery substage occurs at 4.15 K $\pm$ 0.05 K with an activation energy of 0.010 eV $\pm$ 0.001 eV. The I_E substage shifts with defect concentration in lead as it does in copper. The I_E activation energy is 0.010 eV $\pm$ 0.001 eV. Since platinum and lead anneal in Stage I in the normal fashion, the strange behavior of gold is not clearly determined by its position in the periodic table.

ACKNOWLEDGMENTS

I would like to thank Professor J. S. Koehler for suggesting this project and for his guidance and support.

I would also like to thank the faculty, students and staff of the University of Illinois who assisted me in this work. A special note of thanks goes to Dr. Y. N. Lwin for the loan of the computer data acquisition system.

This research was supported by the U. S. Atomic Energy Commission under contract AF(11-1)-1198.

TABLE OF CONTENTS

I. INTRODUCTION

The low temperature recovery of the radiation induced damage in the face-centered-cubic metals has been characterized by two types of behavior.[1] For the group of copper, silver, platinum and aluminum, irradiation with electrons at sufficiently low temperatures produces crystal damage in the form of equal numbers of stable interstitials and vacancies. Upon warming the damage in these materials is removed in distinct recovery stages. For the case of the "normal" fcc metals the lowest temperature recovery, Stage I, contains five substages. The temperatures of the four lowest substages are independent of the defect concentration and are associated with the recombination of an interstitial with its own vacancy. The fifth substage shifts to lower temperature with increasing amount of damage and is associated with free long range migration of interstitials through the lattice to vacancies and to other sinks such as impurities or dislocations. In the case of copper, Stage I occurs between 15 K and 55 K. For electron irradiation of copper, about 85% of the resistivity increase introduced on irradiation anneals in Stage I.

The second type of behavior has been found only in the case of gold. Here the radiation induced damage recovers more or less continuously as the temperature is increased starting as low as 2 K.[2] It appears that the gold interstitial can undergo long range migration at or below 2 K. For gold only about 25% of the resistivity increase anneals at temperatures below 30 K.

The present experiment was undertaken to determine the radiation damage characteristics of the fcc metal lead which is in the same row of

the periodic table as gold. The low temperature recovery of the electrical resistivity following electron irradiation of lead[3] is found to be very similar to that of copper except that the Stage I recovery in lead occurs between 1.6 K and 5.5 K. Of the fcc metals showing "normal" behavior, this is the lowest Stage I temperature observed.

II. EXPERIMENTAL PROCEDURE

A. Cryostat

1. Dewar

The commercial 10 liter dewar and the vacuum housing are shown in Figure 1. Also shown are the electrical and vacuum plumbing connections. The locations of the refrigerator assembly and the sample chamber are indicated in Figure 2.

2. Refrigerator

The superfluid helium refrigerator is shown in Figure 3. It operates on the principle that the temperature of liquid helium is lowered as the pressure of the gas above the liquid is lowered. Below 2.184 K helium is in the superfluid state. In this state the thermal conductivity and the heat capacity are very large. The superfluid provides effective sample cooling during the electron irradiation.

As the temperature of the liquid helium is lowered from 4.2 K to 1.35 K by pumping, the volume of liquid remaining decreases by 40%. Thus it is necessary to refill the refrigerator while it is operating. This is accomplished by the use of a needle valve. When open the needle valve allows liquid helium at atmospheric pressure to flow from the 10 liter helium dewar into the refrigerator. In series with the needle valve is an impedance tube which supports the pressure difference between the dewar and the refrigerator. The impedance tube is shown in Figure 4. It consists of a #24 (0.5 mm) chromel A wire inside of a cupronickel capillary tube (0.8 mm O.D. × 75 μm W.).

Figure 1. Exterior cryostat assembly. (A) commercial 10 liter helium dewar with 2" neck; (B) vacuum housing with vacuum common to dewar; (C) gate valve; (D) Flange to accelerator; (E) beam direction; (F) flange containing 50 μm aluminium scattering foil; (G) drift tube; (H) radiation shield, insulated from the vacuum housing; (I) Faraday cup, insulated from the vacuum housing; (J) atmospheric vent manifold for helium dewar; (K) refrigerator manifold thermally isolated from the vent manifold by the stainless steel pump out tube (R_a); (L) vacuum feed through of all wires except potential leads; (M) to helium pump; (N) tube for thermal isolation of voltage contact can; (O) voltage contact can; (P) needle valve; (Q) wires.

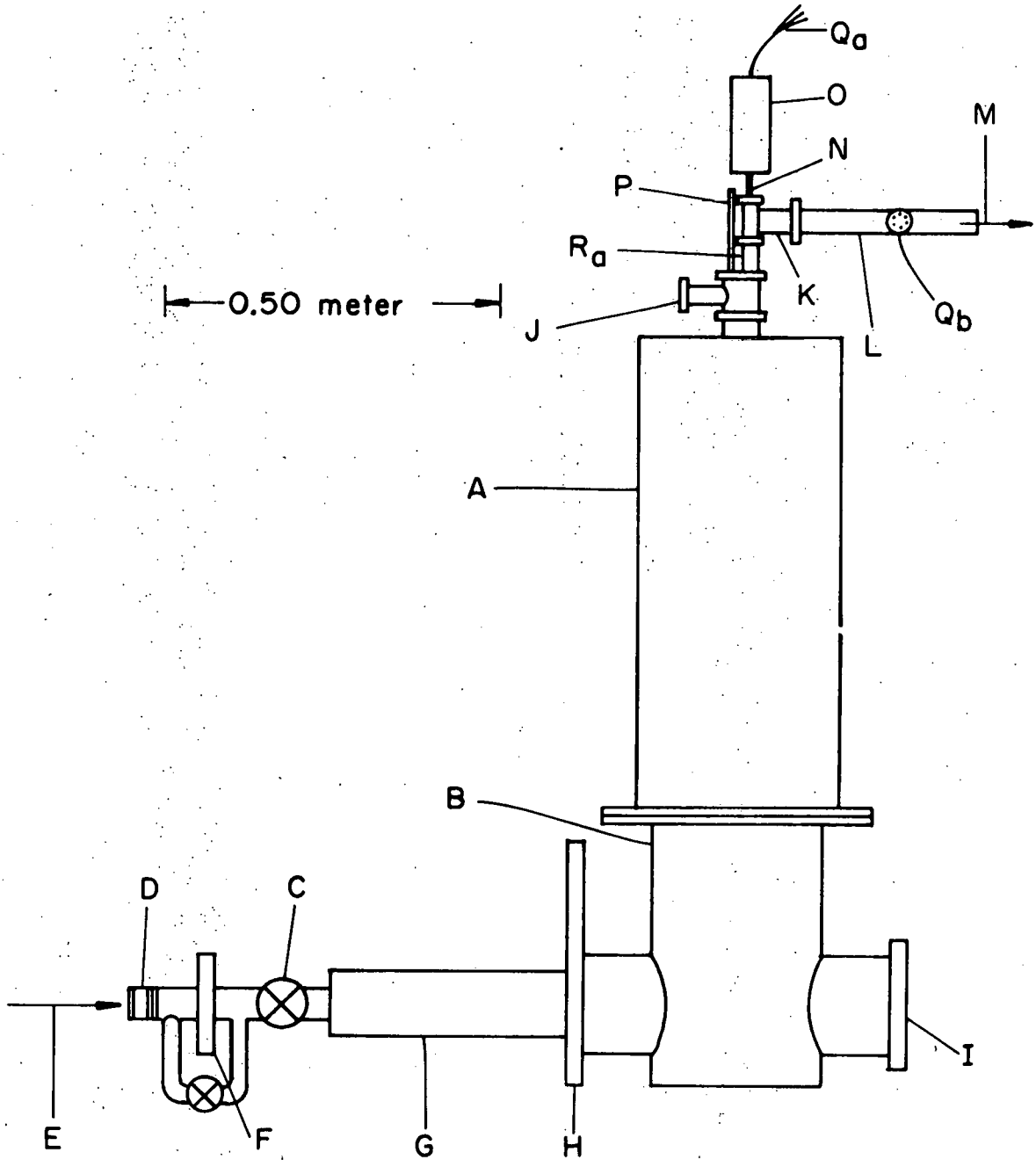
Qa
O
M
N
P
Ra
K
Qb
0.50 meter
J
L
A
B
D
C
E
F
G
H
I

Figure 2. Cross section of cryostat assembly. (A) commercial helium dewar; (B) vacuum housing; (H) radiation shield; (I) Faraday cup; (P) needle valve; (R) refrigerator assembly; (S) sample chamber; (T) LN_2; (U) LHe; (V) 78 K radiation shield; (W) 4.2 K radiation shield.

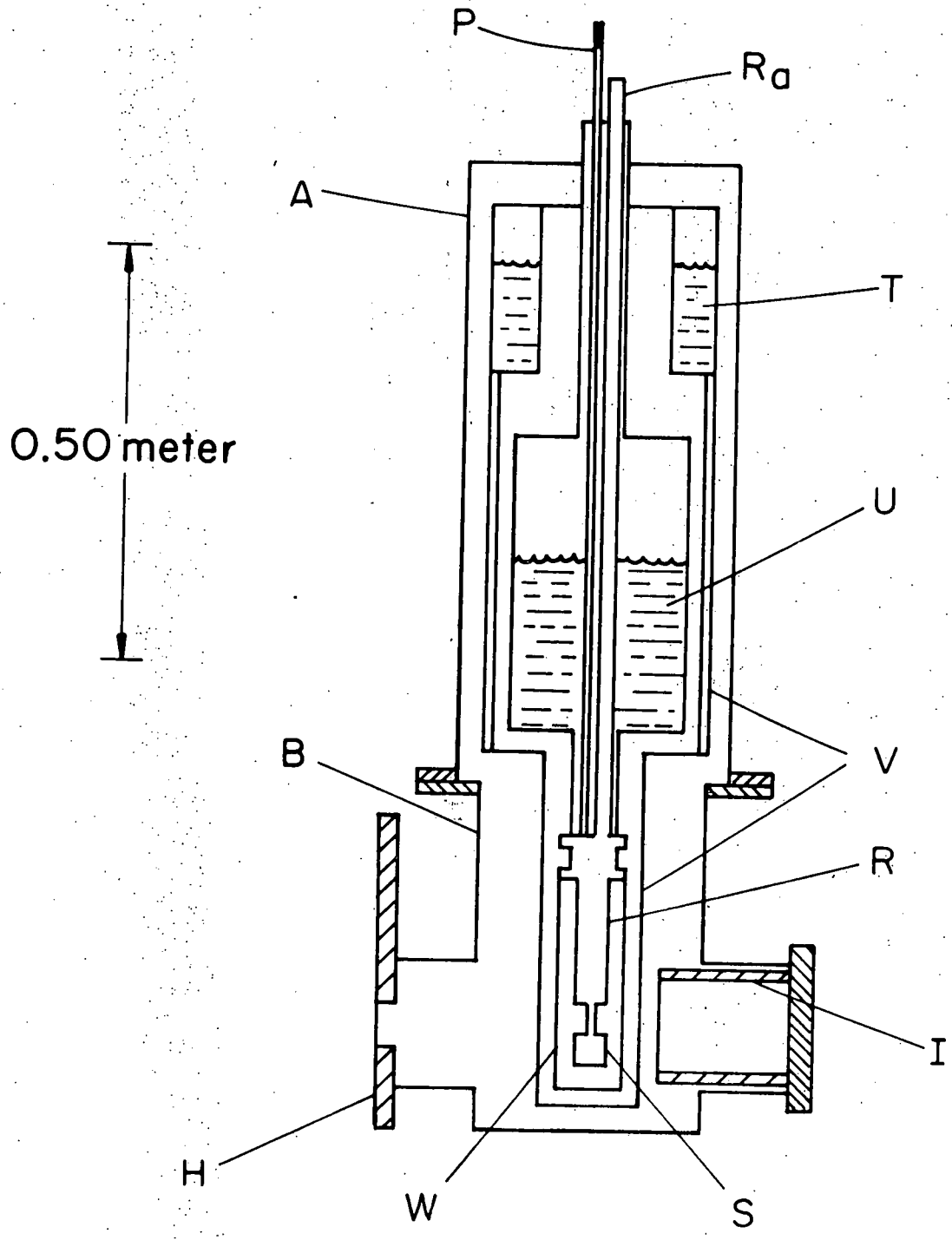
P
Ra
A
T
0.50 meter
U
V
B
R
I
H
W
S

Figure 3. Refrigerator assembly seen in cross section. (A) radiation baffles; (B) pump out tube; (C) needle valve drawn with the threading and male piece omitted for clarity; (D) In o-ring flange; (E) thermal isolation section; (F) upper thermal grounding post; (G) needle valve seat; (H) impedance tube; (I) lower thermal grounding post; (J) liquid reservoir.

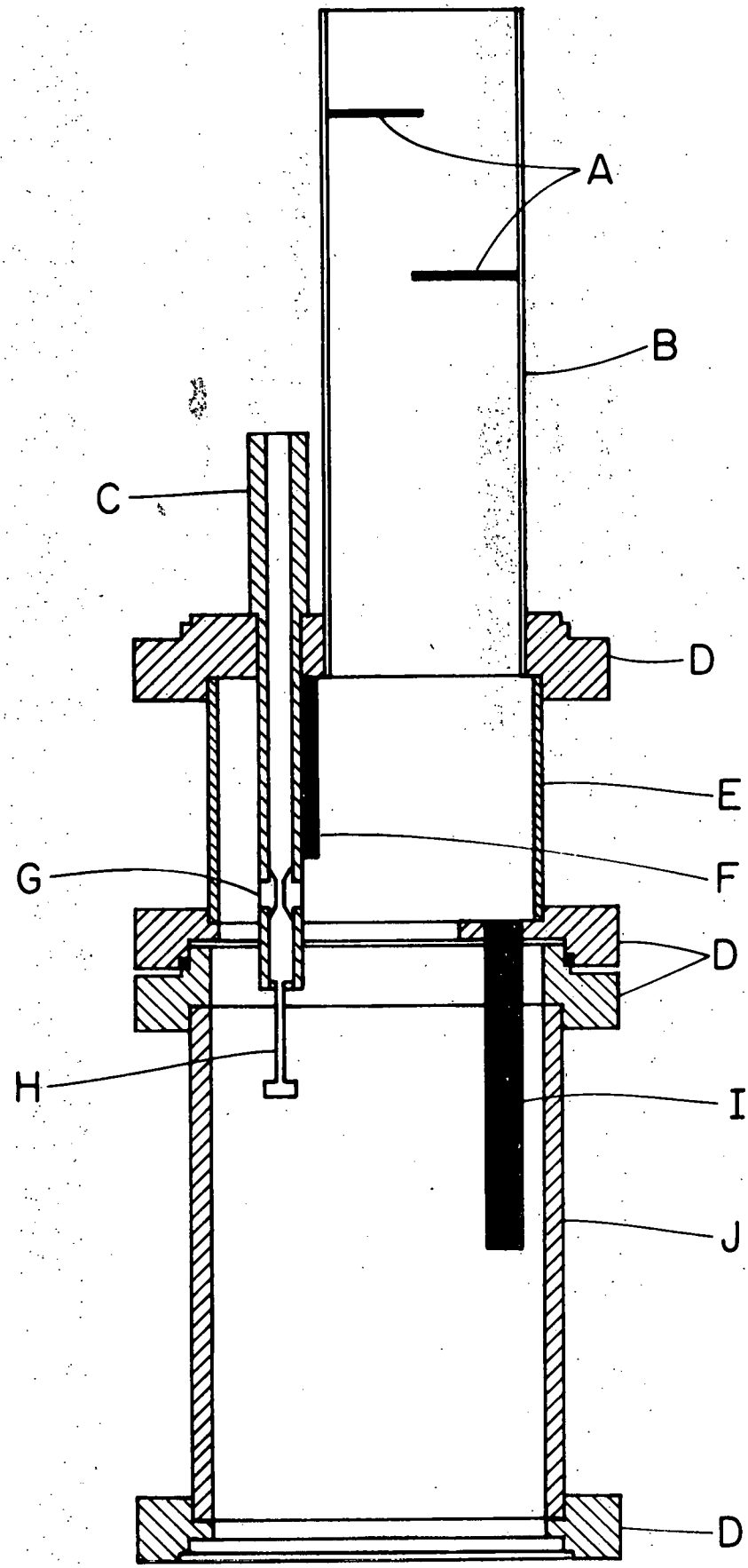
A
B
C
D
E
F
G
D
H
I
J
D

Figure 4. Cross section sketch of impedance tube. See text for dimensions. (X_a) base of needle valve; (X_b) copper plug; (X_c) cupronickel capillary tube; (X_d) chromel wire; (X_e) stainless steel shield tube; (X_f) copper nozzle. All parts soft soldered together except chromel wire left loose.

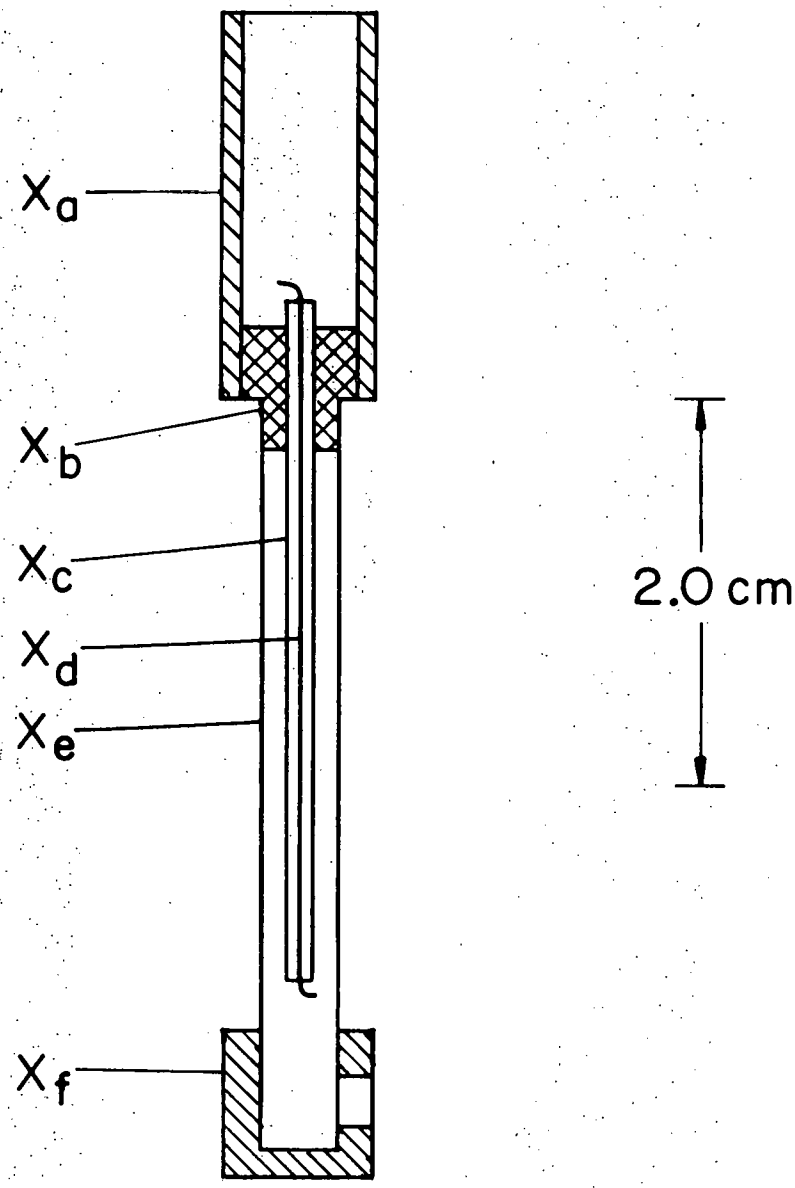
X_a
X_b
X_c
X_d
X_e
X_f
2.0 cm

With a proper needle valve opening and impedance tube, it was possible to operate the refrigerator in a continuously refilling mode and maintain a refrigerator filled with superfluid at a temperature of 1.35 K. The needle valve could be remotely adjusted during the irradiations to maintain a temperature at or below 1.5 K. Since the impedance tube isolates the refrigerator from the liquid helium dewar, it was possible to maintain the equilibrium temperature of 1.35 K while refilling the 10 liter liquid helium dewar.

A 1.25" pump-out tube passes from the refrigerator through the liquid helium dewar. The pump-out tube is connected to a 26 liter/second mechanical pump by 1.5" tubing. A 1" valve is used to throttle the pump.

A stainless steel spacer section is used to isolate thermally the refrigerator from the liquid helium dewar. All sections are connected by indium o-ring seals.

All electrical leads from the sample can pass out through the refrigerator pump-out tube after being thermally connected with GE 7031 varnish to a gold plated copper binding post on the bottom of the liquid helium dewar. All voltage leads pass continuously out of the refrigerator pump-out tube vacuum at room temperature.

A gold plated copper rod hangs from the bottom of the isolation section into the refrigerator. Two 470 Ω 1/8 watt Allen-Bradley carbon resistors are mounted at the top and bottom of this rod. These resistors are used in an external resistance bridge and serve as superfluid helium level indicators. During the irradiations the level of

the superfluid was maintained near the top of the refrigerator.

3. Sample Can

Directly below the refrigerator is the sample can shown in Figure 5. The electron beam enters the sample can through a 0.002" thick aluminum window epoxied (Shell Epon 828 resin and Versimad 125 hardner) over a 0.5" × 0.75" rectangular hole in the copper sample holder. A similar arrangement allows the electron beam to exit the sample can. The electron beam passes through a total of 0.25" of superfluid helium.

Superconducting solenoids are located above and below the sample region. The magnets are wound with 300 turns of superconducting wire supplied by Norton Supercon Inc. The wire has a 0.010" diameter niobium core, 0.0015 copper cladding and a 0.0005" formvar insulation layer, The leads to the magnet are #16 copper wire and are soldered with lead tin solder to the copper cladding of the superconducting wire. Calculations show that the magnetic field varies by less than 4% across the sample area.

The samples were centered in the axial plane of the magnet perpendicular to the irradiating beam by two thin gold plated copper stand offs varnished to the aluminum window outside of the irradiated area. A 200 Ω 1/8 watt Allen-Bradley carbon resistor wrapped with fine copper wire is mounted with GE 7031 varnish on the sample holder adjacent to the samples but out of the irradiated area.

A resistance heater is wound on the outside of each magnet chamber.

Figure 5. Sample chamber. (A) In o-ring flange; (B) superconducting magnet chamber; (C) heater; (D) carbon resistance thermometer; (E) samples; (F) sample mounting plate; (G) 0.002" aluminum beam window.

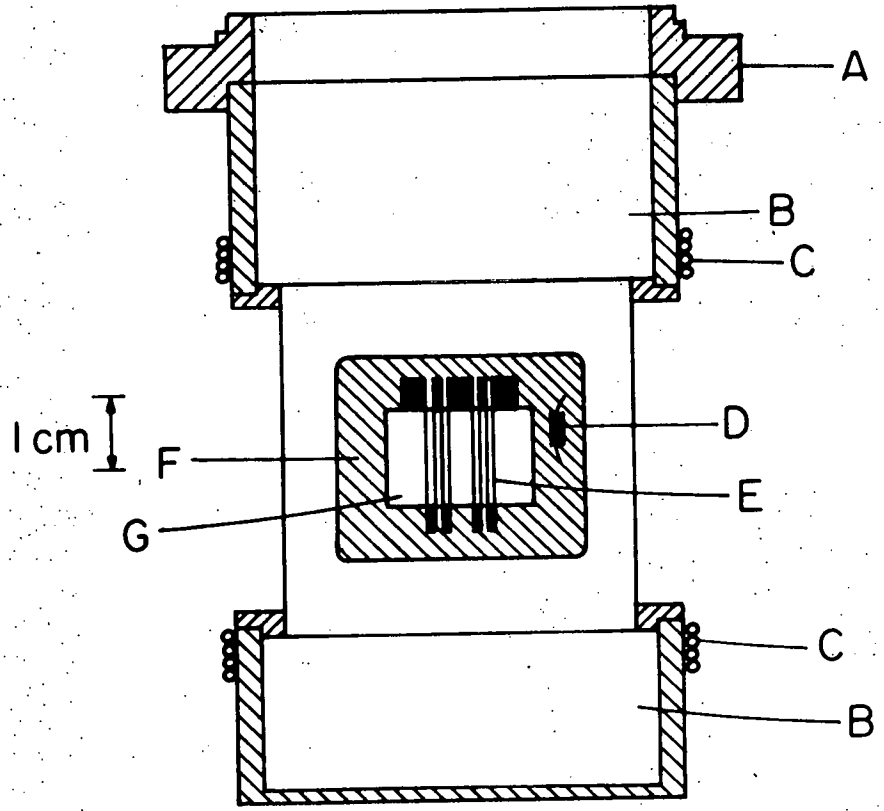
A
B
C
D
E
F
G
1 cm
C
B

B. Irradiation Beam

The electron irradiations were done using a High Voltage Engineering van de Graaff accelerator. Electrons energies of 1.5 MeV were stable to better than 0.01 MeV. The beam was magnetically deflected 90° to provide even greater stability. The beam transport system after the bending magnet is shown in Figure 6. A 0.002" aluminum foil separates the accelerator and cryostat vacuums and serves as a scattering foil to provide greater spacial uniformity of the electron beam. For the foil, electron multiple scattering theory[4] predicts a Gaussian angular distribution of the beam. The angle at which the distribution has 1/e of its maximum intensity is 4.9°. The beam is reduced to the size and shape of the sample can window by collimators attached to the nitrogen and helium temperature shields. Aluminum foils of 0.0005" thickness cover each of the collimators. The collimators were optically aligned with the use of cross-hairs. The window on the sample can is a 0.002" aluminum foil.

The beam uniformity in both the vertical and horizontal directions was measured by the use of shutters and found to be better than 10% across both samples. The total energy loss before reaching the samples was calculated[5] to be about 0.15 MeV. The energy loss in the samples was calculated to be 0.10 MeV.

After passing through the sample can the electron beam is collected in a Faraday cup which accepts all electrons making angles of less than 45° with the center of the sample window. The mean scattering angle for the lead samples is calculated to be 86°. Since the

Figure 6. Beam collimation system. (A) 0.002" aluminum scattering foil; (B) radiation shield; (C) shutters; (D) room temperature collimator; (E) 0.0005" aluminum window; (F) liquid nitrogen temperature collimator; (G) 0.0005" window; (H) liquid helium collimator; (I) two samples with the sample chamber omitted; (J) Faraday cup. All collimators are 0.5" thick.

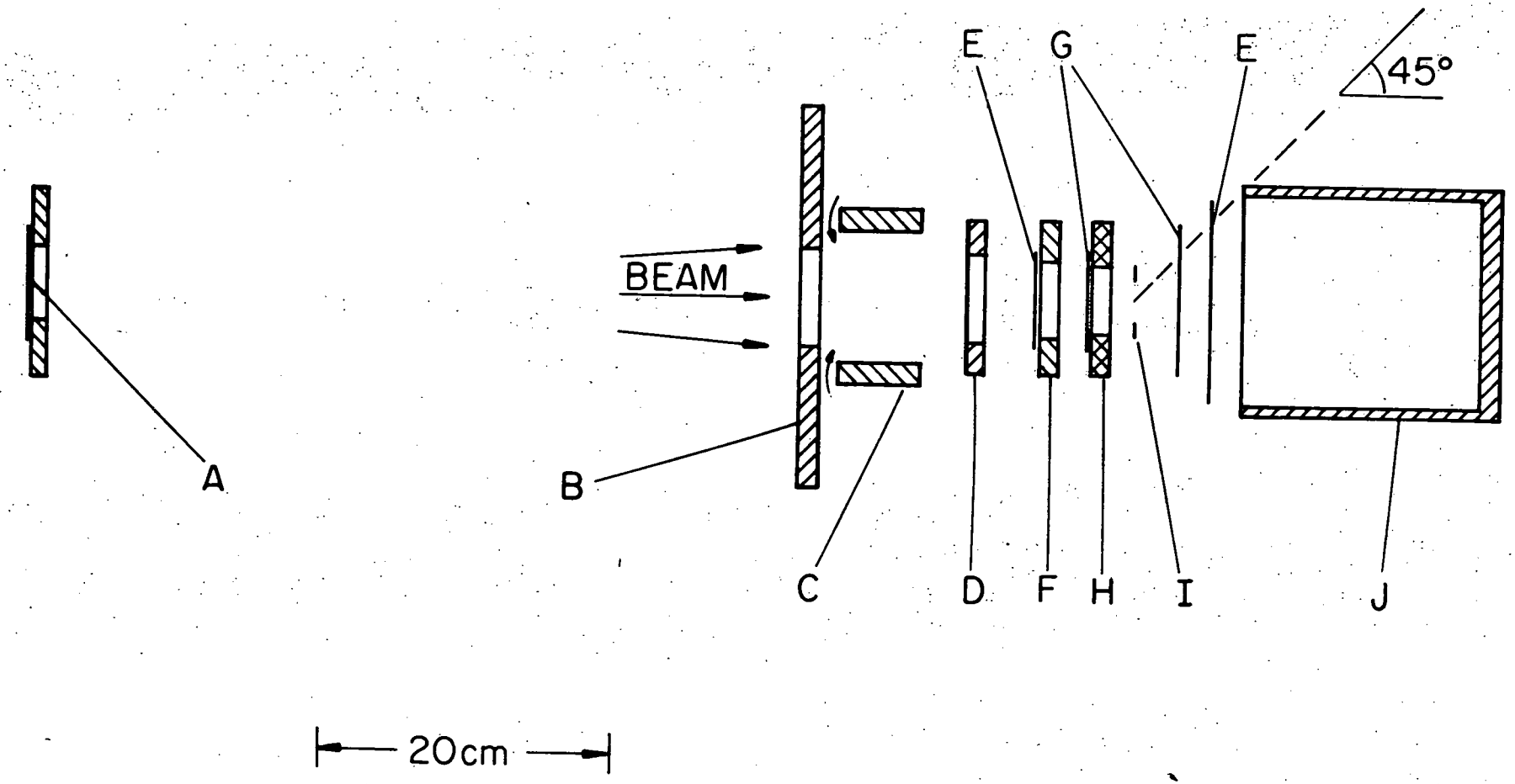
A
BEAM
B
C
E
G
E
45°
D
F
H
I
J
20cm

samples obstruct about 1% of the beam, 9% of the beam will escape detection in the Faraday cup.

C. Sample Preparation

Lead foil of 0.005" thickness was supplied by Cominco American. The starting material was 6-9's grade; spectographic analysis after rolling into sheets showed 0.7 ppm Si, 0.6 ppm Fe, 0.5 ppm Al, 0.5 ppm Ca. The sheets were cut into samples of the shape shown in Figure 7a by an electric discharge machine using a tungsten electrode in clean oil. Mass spectrographic analysis at the University of Illinois Materials Research Laboratory's Spectrographic Laboratory showed no change in the impurity content of the samples due to the electric discharge cutting. The samples were etched in warm dilute nitric acid.

The final sample thickness was 0.003" to 0.004". Small tinned copper leads were spot welded to the samples and the samples were mounted on the sample holder with GE 7031 varnish. Electrical insulation was provided by a 6 μm mylar film. After mounting and air drying at room temperature, the support strips were cut away with a blade to produce the sample shape shown in Figure 7b. After mounting the sample holder on the sample can, current and potential leads were soldered to the spot welded sample leads. It was necessary to spot weld leads to the samples as direct soldering introduced impurities into the samples. Such impurities produce a nonlinear magnetoresistance.

The geometric factor which converts the measured electrical

Figure 7. Samples cut by electron discharge machine (a) before mounting, (b) mounted with spot-welded leads.

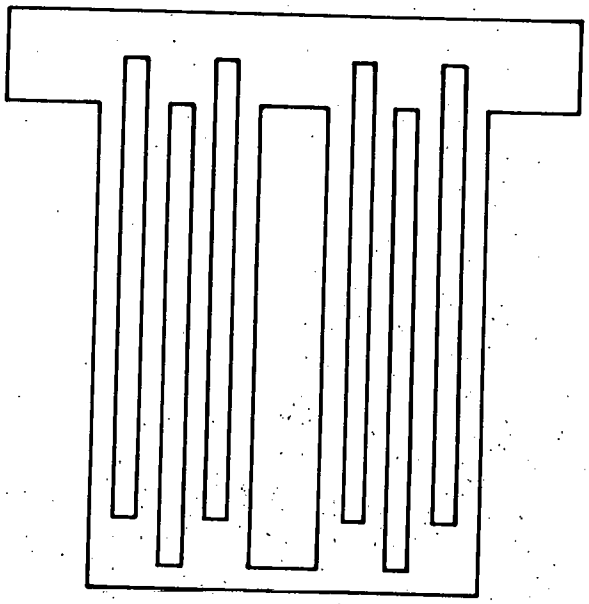

a

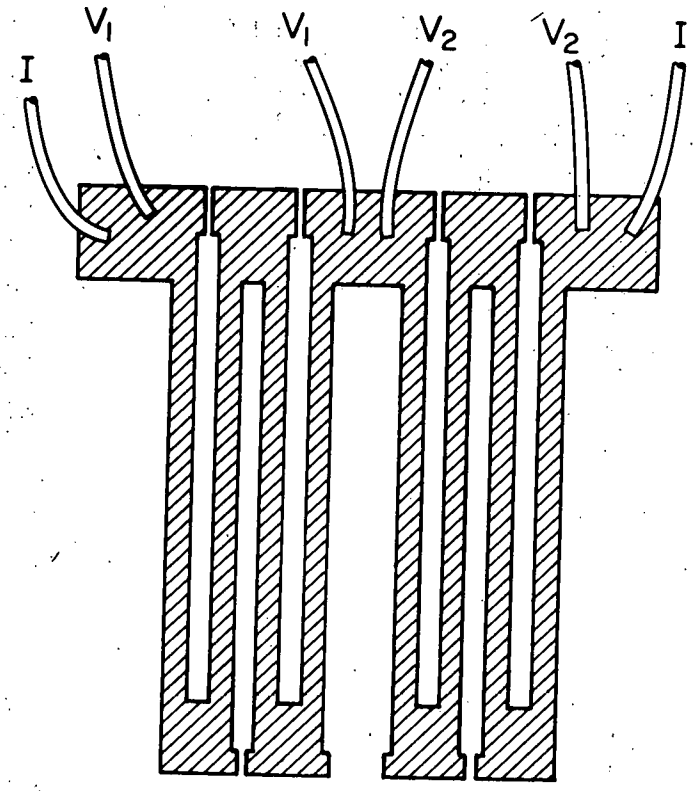

b

resistance (cross section area/length) was obtained for each sample by measuring the resistance at liquid nitrogen temperature and using 4.80 μΩ-cm for the resistivity at nitrogen temperature. The geometric factors were uncertain to 0.01%.

D. Temperature Measurement

Below 4.2 K the temperature of the sample can was determined by measuring the vapor pressure of the liquid helium bath in the sample can and using the 1958 temperature scale[6] to convert the pressure readings to temperature readings. The pressure was measured by two Wallace-Tierman gauges. The first gauge reads from 0 mm to 50 mm pressure, corresponding to temperatures up to 2.29 K. The second gauge was used from 50 mm to 750 mm pressure, corresponding to temperatures up to 4.2 K. Both Wallace-Tierman gauges were calibrated against a Texas Instruments Fused Quartz Precision Pressure Gage (0.01%).

As an additional check on the sample temperature, the 200 Ω Allen-Bradley carbon resistor in the sample can was calibrated under equilibrium conditions at temperatures of 1.3 K to 4.2 K. Standard fitting techniques[7] were used to interpolate temperatures above 4.2 K. The form of the assumed temperature dependence of the resistance of the carbon resistor is

$$[\ln R/T]^{1/2} = A + B \ln R \ , \qquad (1)$$

where R is the resistance, T the temperature, and A and B are fitting constants. For a 10 Ω 1/2 watt Allen-Bradley unit, this fit was found to deviate from the measured relationship by 0.4% in the range 5 K - 25 K.[8]

The thermometer is used to insure that the helium bath temperature corresponds to the pressure in the sample can and to determine temperature above 4.2 K. The error in the calculated value of the superconducting transition temperature of the lead samples was less than 0.1 K.

The effect of the irradiation on the carbon resistor is expected to be negligible. Ohmite resistors exposed to 10^6 rad of γ-irradiation or 2×10^{10} neutrons showed no change at 1 K.[9]

E. Heating

1. Irradiation Temperature

During the electron irradiation the temperature of the samples and the sample can will rise due to energy loss by the electron beam. For an electron with an energy of 1.5 MeV, the mean rate of energy loss in the lead samples is 10 MeV/cm. The total energy loss in each leg of the sample was 2×10^{-5} watt for the maximum irradiation flux of 4×10^{10} e/sec cm^2 used in this experiment. In the steady state, the energy flow through the surface of the sample, 3×10^{-4} watt/cm^2, was much less than the superfluid transfer limit of 1 watt/cm^2 at 1.5 K.[10] Thus the surface of the samples was at the bath temperature. For a round wire with uniform heating, the temperature difference between the center and the surface is given by,

$$\Delta T = \frac{1}{4\pi K} \left(\dot{\varepsilon} / \ell \right) \qquad (2)$$

where K is the thermal conductivity and $\dot{\varepsilon}/\ell$ is the heating per unit length. Using $K = 2$ watt/cm K,[11] the temperature difference is ex-

pected to be 7×10^{-7} K. Therefore, the samples were at the bath temperature.

The electron energy loss in the samples and the liquid helium resulted in a power dissipation of 1.2×10^{-3} watt in the sample can. Another source of heating resulted from the large angle scattering electrons which are then stopped in the sample can. From section II B, about 9% of the electrons were stopped in the sample can. This resulted in a power dissipation of 1.7×10^{-3} watt. The total power dissipation in the sample can was about 3×10^{-3} watt. When 0.1 watt was dissipated in the sample heater, the sample temperature rose to 1.6 K. As a check on the beam heating, two samples were irradiated at one half the normal flux. No change in the low temperature recovery was observed. The sample temperature during the irradiations was always at or below 1.5 K.

2. Measurement Temperature

For a typical sample, the 2 amp sample current produced a power dissipation of 2×10^{-4} watt in the sample. This resulted in a temperature gradient between the center and surface of the sample of 1.6×10^{-6} K. The main bath heating during the measurement was due to the magnet current. This raised the bath temperature to 1.4 K. This was well below the temperature (1.6 K) at which the thermal resistivity of the lead could be detected.

F. Resistivity Measurements

Since lead is in the superconducting state at temperatures below 7.19 K, it is not possible to observe directly the defect re-

sistivity at the measurement temperature of 1.35 K. Thus it was necessary to apply a longitudinal magnetic field to the samples to quench the superconductivity. This technique has been used to study the temperature dependence of the resistivity of lead at temperatures below its superconductivity transition.[12] It was observed that, at magnetic fields above the critical field, the resistivity of polycrystaline lead increases linearly with magnetic field. The extrapolation of this linear dependence to zero magnetic field was taken as the normal state resistivity. In this experiment the extrapolation was done from measurements in magnetic fields of 1.5 to 2 K Gauss.

The resistance of the samples was measured using standard four wire D.C. potentiometric techniques. The current to the samples was supplied by a Fluke 382 A Current Calibrator and was stable to 1 part in 10^6. All voltages were measured with a Vidar 5200 Data Acquisition System. In this system a Vidar 521 integrating digital voltmeter is controlled by a Digital Instrument Corp. PDP 8/L computer. The computer can, using a Vidar 610 Low Level Scanner, select the desired input and store the measured voltage. In the present experiment each resulting voltage was the average of five readings. It was possible to resolve 0.1 μV. Sample resistivities were uncertain to 10^{-12} Ω-cm.

The resistivity of one sample is shown in Figure 8 as a function of the applied magnetic field. In magnetic fields above the critical field, the sample resistance, R, is a linear function of the magnetic field H. As shown in Figure 9 the slope of the sample resist-

Figure 8. Resistivity vs. applied magnetic field.

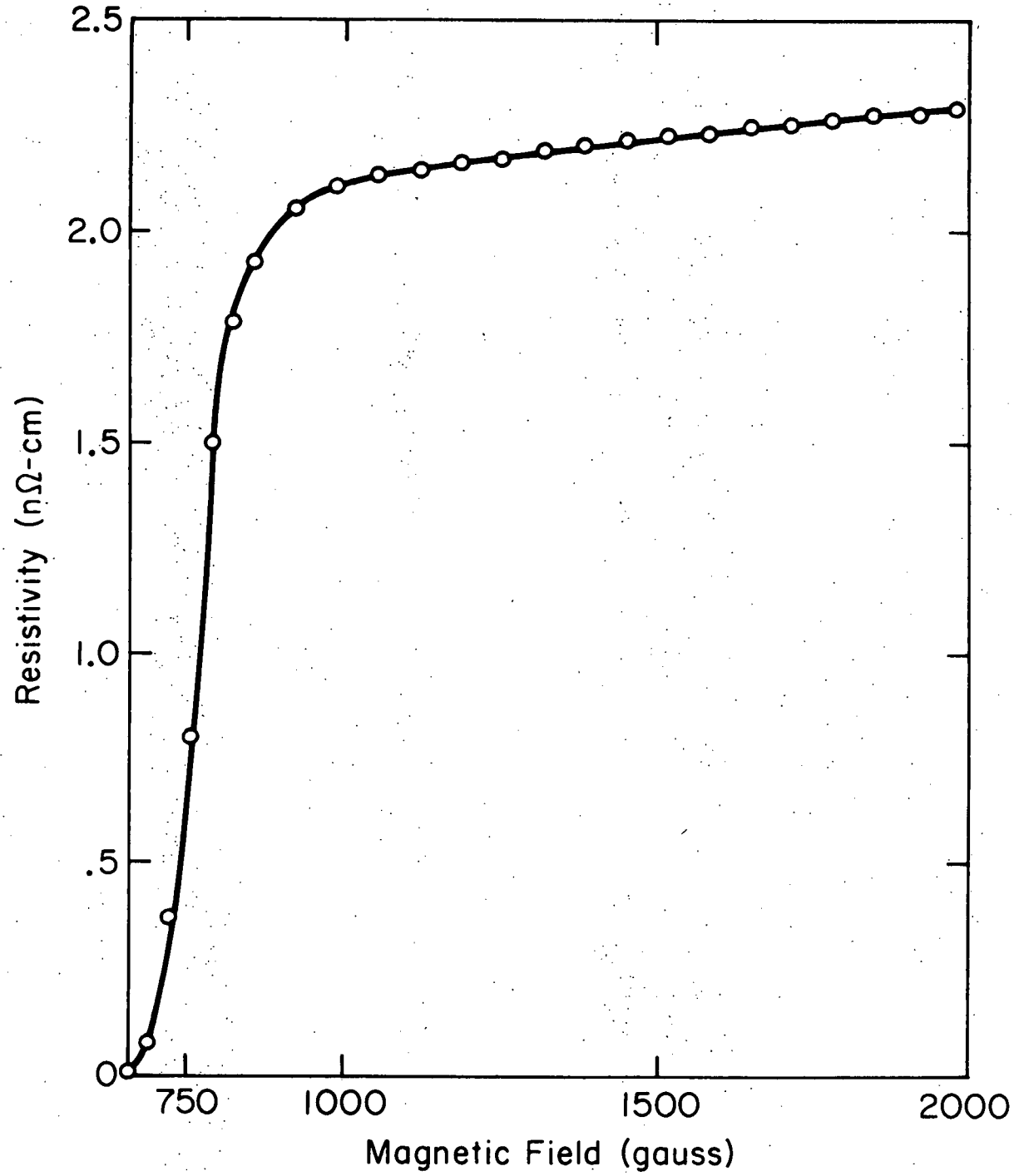
2.5
2.0
1.5
1.0
.5
0
Resistivity (nΩ-cm)
750
1000
1500
2000
Magnetic Field (gauss)

Figure 9. Slope of the resistivity with respect to the magnetic field vs. the resistance at a fixed value of the magnetic field.

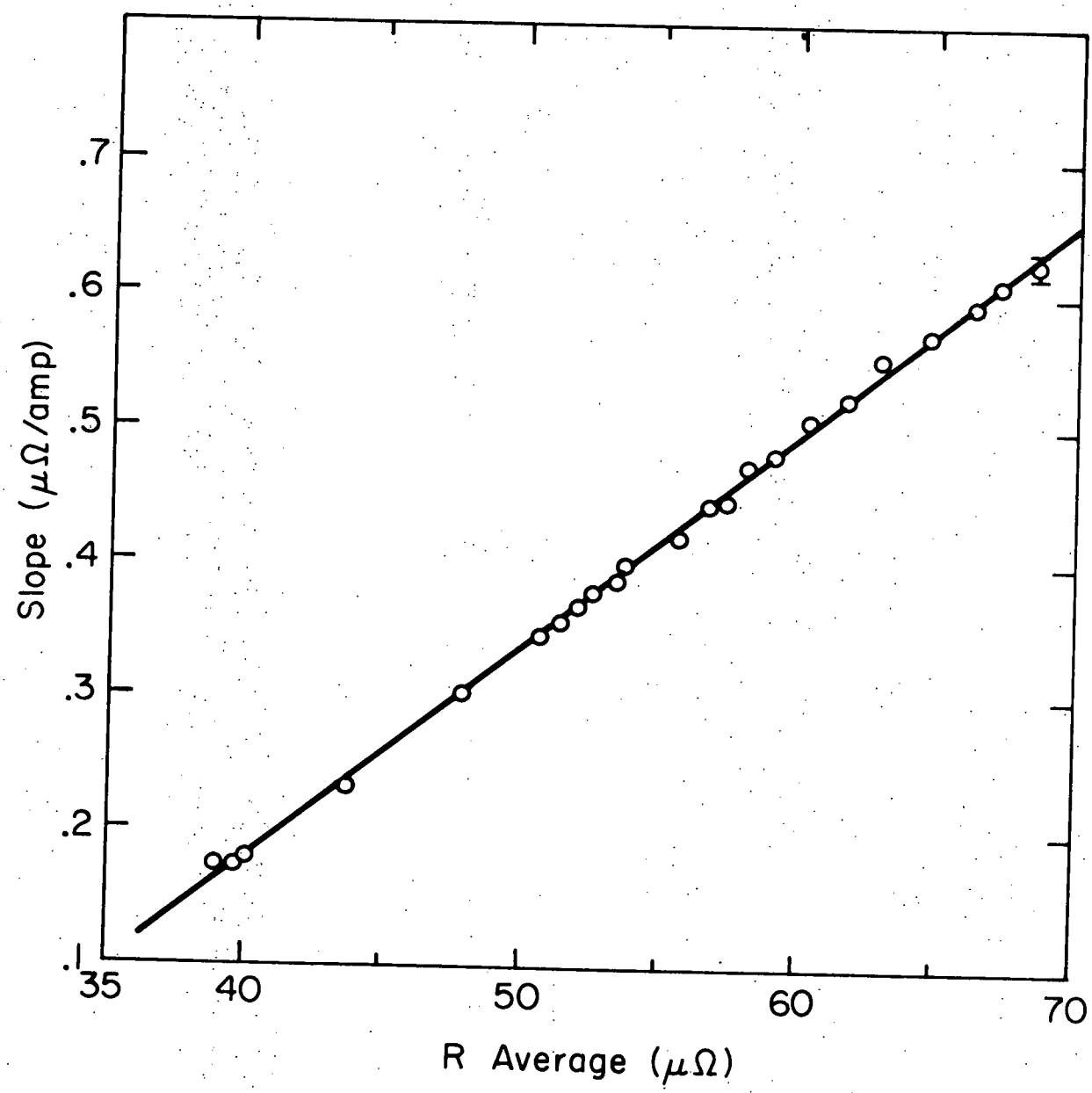
.7
.6
.5
.4
.3
.2
.1
Slope (μΩ/amp)
35
40
50
60
70
R Average (μΩ)

ance with respect to the magnetic field was a linear function of the resistance at a fixed value of the magnetic field. Thus,

$$R(C,H) = R_o(C) + H \cdot \frac{dR(C)}{dH} \tag{3}$$

and

$$\frac{dR(C)}{dH} = S + T \cdot R(C,H_1) \tag{4}$$

where C is the radiation induced defect concentration, R_o is the bulk zero field resistance, and S and T are constants.

The change in slope may result from changes in the magnetoresistivity size effect or a nonlinear dependence of the magnetoresistivity on the defect concentration. Calculations for round wires[13] and thin films[14] show that the size correction decreases as the magnetic field increases or as the mean free path decreases. The mean free path will decrease as the magnetoresistance increases and as the defect concentration increases. These effects change the measured slope of the resistivity verses magnetic field as the defect concentration increased and may cause an apparant decrease in the rate of damage production as the amount of damage increases.

Eqs. (3) and (4) can be solved to yield,

$$R(C,H_1) = \frac{R_o(C) + S \cdot H_1}{1 + T \cdot H_1} \tag{5}$$

where H_1 is the value of the fixed magnetic field. Fractional changes in the radiation induced resistivity can be expressed as fractional

changes in the fixed field resistance,

$$\% \text{ recovery} = \frac{R_o(C) - R_o(0)}{R_o(C_o) - R_o(0)} = \frac{R(C,H_1) - R(0,H_1)}{R(C_o,H_1) - R(0,H_1)} \qquad (6)$$

where C_o is the total radiation induced defect concentration.

Thus the fractional changes in the resistivity can be followed by monitoring the resistance at a fixed value of the magnetic field. This procedure has the advantage of lower noise flucation. The noise flucations are greater in the extrapolated values since the distance over which the extrapolation is made is approximately two and one half times the range over which the sample resistance is measured. Schroeder[15] has reported that for irradiations at 4.7 K the recovery of the zero field extrapolated resistivity and the fixed field resistivity are within 1%.

All absolute resistivities are calculated from the zero field extrapolated resistances. The resistivity was independent of temperature below 1.5 K. All resistivities used to monitor the radiation damage were measured at 1.35 K.

G. Anneals

As the temperature of a damaged sample is raised, the various defects in the sample may become mobile. The temperature is raised by reducing the pumping on the refrigerator, adding helium gas to the refrigerator and passing current through the sample heater. Below 4.2 K care must be taken that the liquid helium bath temperature cor-

responds to the helium gas pressure. The temperature was controlled to better than 0.005 K below 4.4 K and to better than 0.05 K above 4.4 K. Less than twenty seconds was required to raised the temperature from the previous annealing temperature to the desired annealing temperature, and less than one second was required to lower the temperature.

The mobile defects can undergo reactions which change the state of the sample and alter its resistivity. Such reactions are conviently observed in an isochronal annealing experiment. For the isochronal anneals in this experiment the resistivity is measured at the base temperature of 1.4 K. The thermal contribution to the resistivity could not be detected below 1.6 K. The sample is rapidly warmed to the desired annealing temperature for a fixed time of five minutes, rapidly cooled to the base temperature and the resistivity is remeasured. This procedure is then repeated at the next higher temperature.

The time dependence of the defect reactions can be studied in an isothermal annealing experiment. In this experiment the sample was repeatedly annealed to the same temperature with resistivity measurements at the base temperature between anneals. Once the time dependence of the recovery was established at the first temperature the same process was repeated at the next higher annealing temperature.

For a single thermally activated process, the isothermal data may be analyzed by the change in slope between two successive temperatures.[16] In this analysis the resistivity is assumed to be

proportional to the concentration of defects and to recover according to a monomolecular rate equation of the form

$$\frac{d\rho}{dt} = \dot{\rho} = -\nu f(\rho) e^{-E/kT} , \qquad (7)$$

where ν is the pre-exponential frequency factor, $f(\rho)$ is some function of the resistivity ρ, and E is the thermal activation energy for the recovery process. For a simple rate equation, $f(\rho)$ is given by ρ^n, where n is the order of the kinetics of the defect reaction. If the time derivative of the recovery is measured at the same resistivity for two different temperatures, then the activation energy is given by

$$E = k \frac{T_1 T_2}{T_2 - T_1} \ln(\dot{\rho}_2/\dot{\rho}_1) \quad . \qquad (8)$$

III. EXPERIMENTAL RESULTS AND ANALYSIS

A. Damage Production

The production of damage for three irradiations with 1.5 MeV electrons on one sample is shown in Figure 10. The initial production rate is 7.4×10^{-25} Ω-cm^3/e. It falls to 4.3×10^{-25} Ω-cm^3/e at 1 nΩ-cm of damage. This decrease may result from size effects in the electrical resistivity or from the fact that the resistivity is not a linear function of the defect concentration. The uncertainty in the production rate due to beam inhomogeneity is 10%. The data may be compared to the value of 1.5×10^{-25} Ω-cm^3/e at 1 nΩ-cm for 1.2 MeV electrons reported for an irradiation at 4.7 K.[13] Since approximately 50% of the damage is removed by annealing to 5 K following an irradiation at 1.5 K, the two values are seen to be roughly consistent with each other.

The production rate was observed to fall to zero for electrons with an estimated energy of less than 0.69 ± 0.03 MeV at the samples. This gives a value of 12.1 ± 0.7 eV for the threshold energy for displacement of an atom from its lattice position. For electron irradiations at 4.7 K the threshold has been found to be 12.5 ± 1.2 eV.[10]

The 1.50 MeV electrons struck the sample with an estimated energy of 1.35 MeV. These electrons could transfer a maximum energy of 30.0 eV to a lead atom. Since the sample thickness was much less than the range of the electrons, the electrons are expected to produce isolated interstitial-vacancy pairs that are homogeneously distributed through the sample.

Figure 10. Change in the resistivity vs. integrated flux for three different irradiations with 1.5 MeV electrons on one sample below 1.5 K. The sample was annealed to room temperature between irradiations.

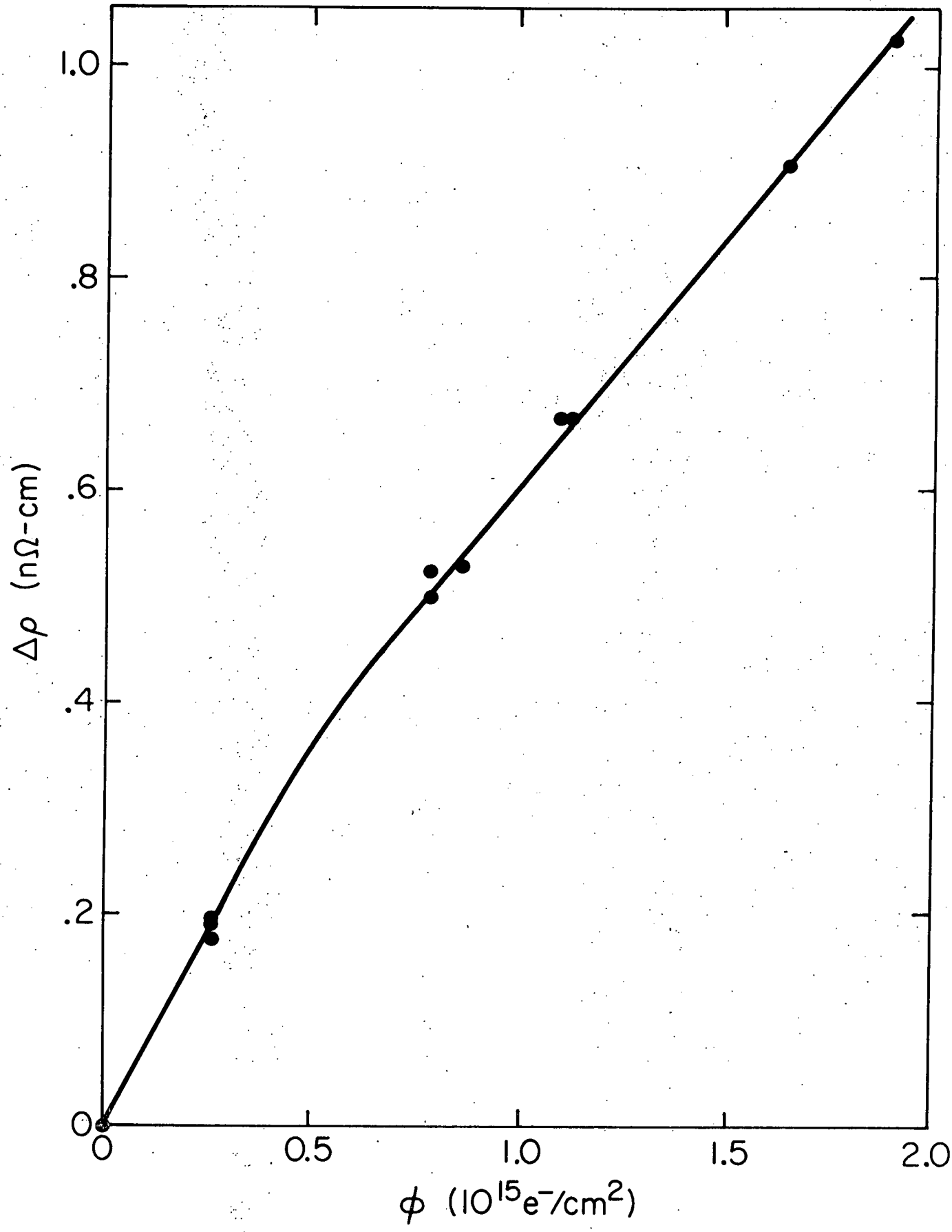
1.0
.8
.6
.4
.2
0
0
0.5
1.0
1.5
2.0
Δρ (nΩ-cm)
φ (10^15 e^-/cm^2)

B. Isochronal Annealing

The results of three isochronal annealing experiments on the same sample are shown in Figure 11. The anneals followed irradiations at 1.5 K with 1.50 MeV electrons. The measured radiation induced resistivity changes were 0.122, 0.523 and 1.03 nΩ-cm. The sample was annealed to room temperature between irradiations. The derivative with respect to temperature of the isochronal recovery is shown in Figure 12 for one sample with measured initial resistivity changes of 0.122 and 1.03 nΩ-cm and for a second sample with a resistivity change of 0.554 nΩ-cm. The derivatives were calculated by finding the slope of a straight line between adjacent isochronal annealing points.

The low temperature recovery stage contains five substages. The four lowest temperature recovery substages appear to be independent of the concentration of radiation induced defects while the highest temperature substage shifts to lower temperature with increasing defect concentration. This structure is similar to that observed following a low temperature irradiation of copper.[1] Accordingly, the recovery below 5.5 K in lead will be labeled Stage I. Stage II begins with a recovery stage at about 5.9 K.

The total annealing in the I_A, I_B, and I_C substages in lead is less than 5%. Thus the derivatives of these substages are not experimentally determined with great precision. The I_A substage occurs in the temperature range of 1.7 K to 2.0 K. The recovery in this substage was always less than 1% of the total radiation damage. The flux used in the 0.122 nΩ-cm irradiation was reduced to one half the

Figure 11. Recovery of the resistivity vs. temperature for isochronal anneals on one sample with initial measured resistivity changes of 0.122 nΩ-cm, 0.523 nΩ-cm, and 1.03 nΩ-cm. The sample was annealed to room temperature between irradiations.

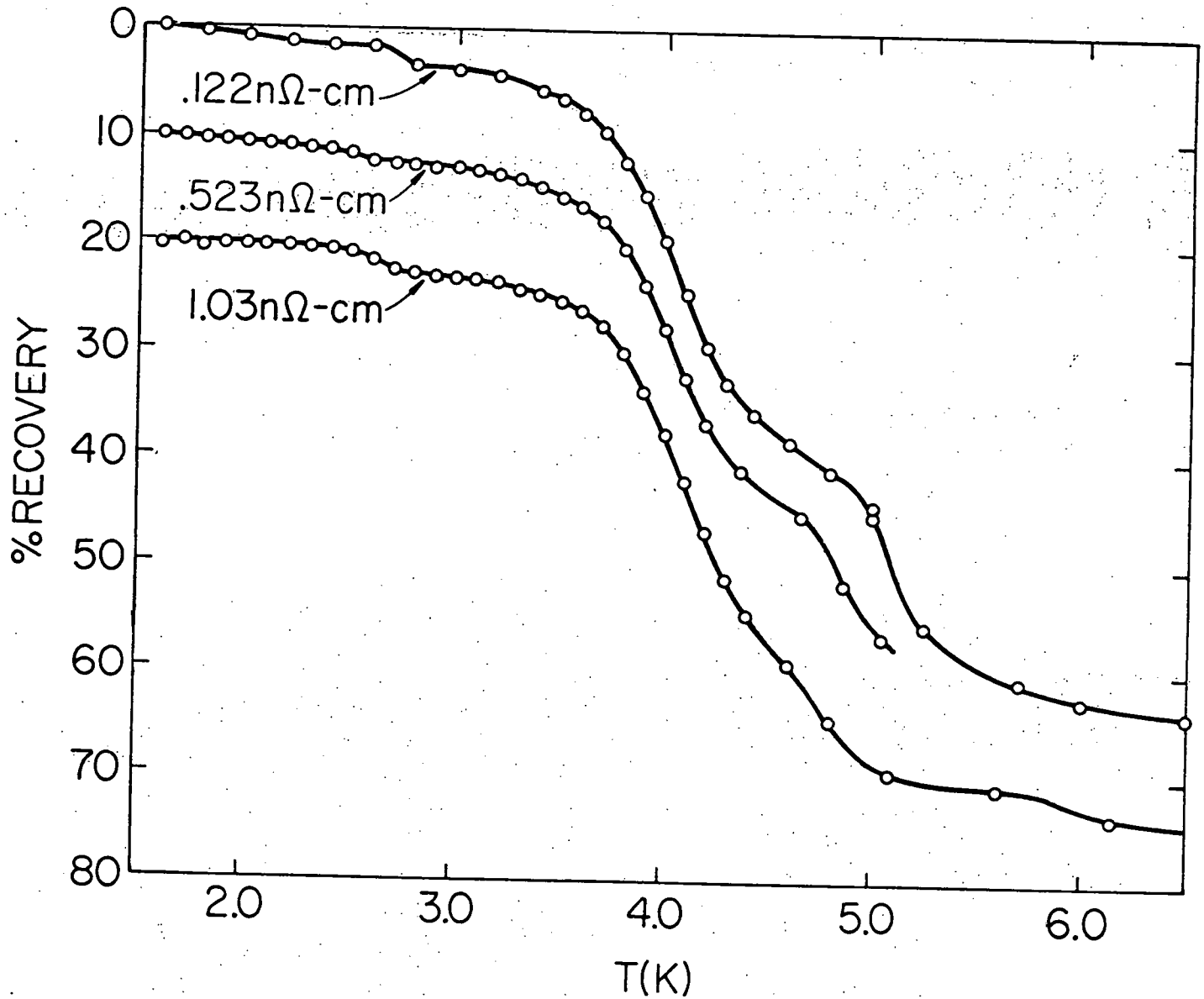
0
10
20
30
40
50
60
70
80
%RECOVERY
.122nΩ-cm
.523nΩ-cm
1.03nΩ-cm
2.0
3.0
4.0
5.0
6.0
T(K)

Figure 12. The rate of recovery of the resistivity with respect to temperature vs. temperature for the sample of Figure 11 with initial measured resistivity changes of 0.122 nΩ-cm and 1.03 nΩ-cm and a second sample with an initial measured resistivity change of 0.554 nΩ-cm.

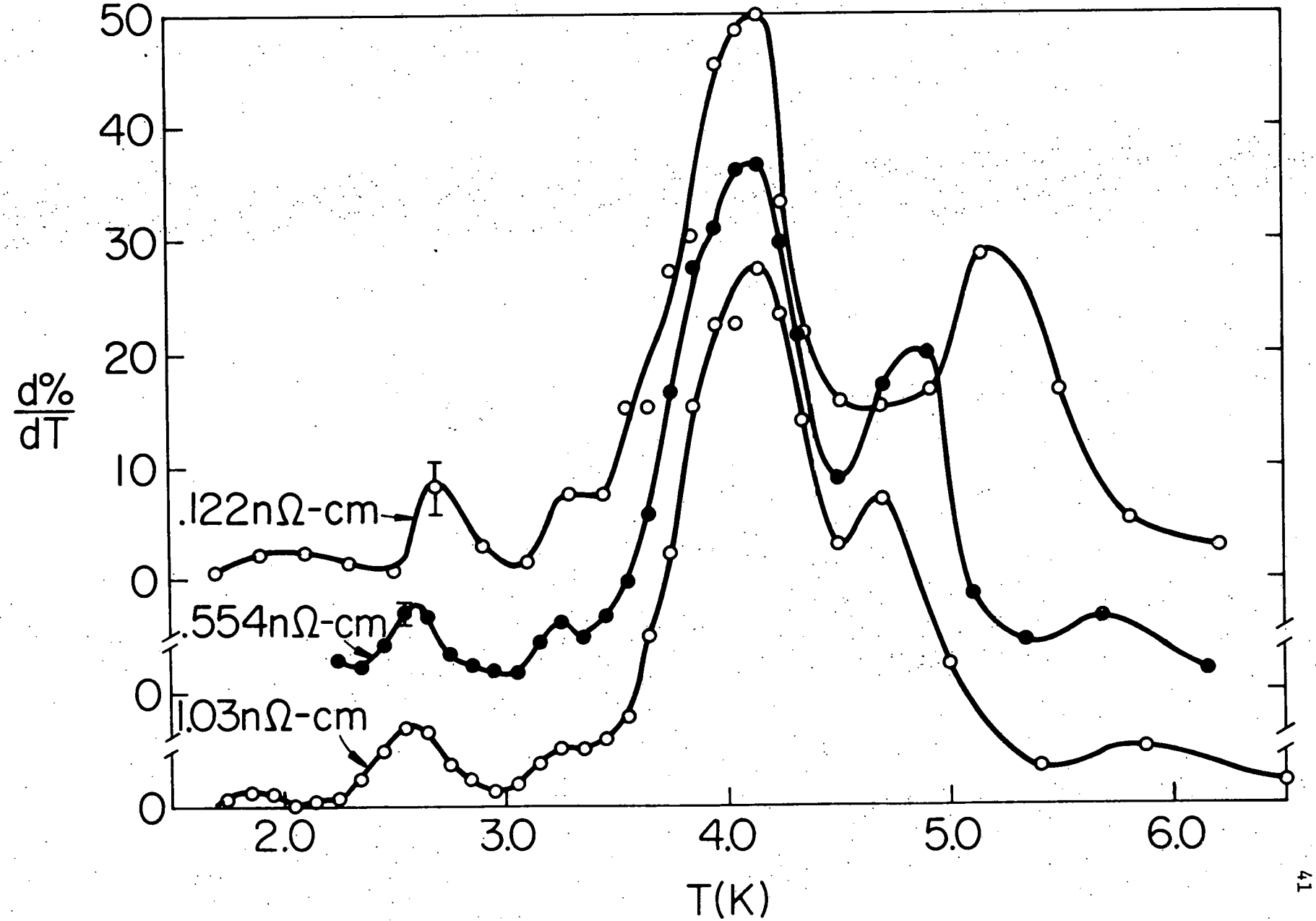
50
40
30
20
10
0
0
0
d%/dT
.122nΩ-cm
.554nΩ-cm
1.03nΩ-cm
2.0
3.0
4.0
5.0
6.0
T(K)

flux used in other irradiations. The temperature during this irradiation was below 1.45 K. The lower irradiation temperature did not result in any change in the I_A substage.

To investigate the effect of subthreshold collisions on the radiation damage, a sample was initially irradiated with 1.5 MeV electrons to a fluence of 5.2×10^{14} e/cm^2 at a temperature of 1.45 K followed by an irradiation at 1.4 K with subthreshold electrons of energy of 0.52 MeV to a fluence of 1.3×10^{14} e/cm^2. The subthreshold irradiation produced a recovery of $0.5 \pm 0.25\%$. This recovery is equivalent to the I_A substage. It is believed that the I_A substage is reduced during the irradiation by subthreshold collisions. This effect has also been observed for the I_A substage in platinum.[16]

The I_B recovery substage is an isolated recovery stage centered at 2.6 K with a half width of 0.35 K. For all irradiations, the recovery in this substage varied between 2.4% and 2.9% with no consistant dependence on the irradiation dose. The apparent shift in the temperature of the I_B peak for the 0.122 nΩ-cm irradiation is due to the reduced resolution in the measurement of the recovery (0.5%) for this low dose and to the use of larger temperature steps between the isochronal anneals.

The I_C substage appears as a low temperature shoulder on the I_D substage. The recovery in this substage begins at 3.0 K. About 2% of the total radiation induced damage is removed in the I_C substage.

The main recovery begins in the I_D substage. The maximum rate of recovery for the I_D substage occurs at $4.15 \text{ K} \pm 0.05$ K. The

recovery in this stage removed about 40% of the radiation damage.

The final substage, I_E, is strongly dependent upon the concentration of defects. The defect concentration dependence of this recovery will be discussed in section III D.

There appears for some samples a recovery stage at about 5.8 K. The total recovery in this stage for the 1.03 nΩ-cm irradiation is 2.5%. The same recovery has been observed[10] at 5.6 K following electron irradiation at 4.7 K. The recovery for a 1.0 nΩ-cm irradiation at 4.7 K was about 9% of the total radiation damage. Since at least 50% of the damage has recovered below 5.0 K in the present experiment, the two recoveries are seen to be in rough agreement. This recovery marks the beginning of Stage II.

C. Isothermal Annealing

The time dependence of the recovery of the radiation induced damage at a constant temperature is shown in Figure 13 for two samples after irradiation to doses of 0.67 nΩ-cm. The recovery as a function of time is shown for anneals at successive temperatures of 3.5 K (following a five minute anneal at 3.0 K), 3.8 K, 4.0 K, 4.2 K, and 4.4 K. The anneals were done using a pulse method with the remaining resistivity measured at 1.35 K after each pulse. Correction to the time of each pulse for the heating phase was less than fifteen seconds. Total cooling times were less than one second.

The first isothermal anneal at 3.5 K is complicated since it involves the I_C recovery substage and the beginning of the I_D recovery substage. The anneals at temperatures of 3.8 K, 4.0 K, and 4.2 K involve

Figure 13. Recovery of the resistivity vs. time for two samples annealed together.

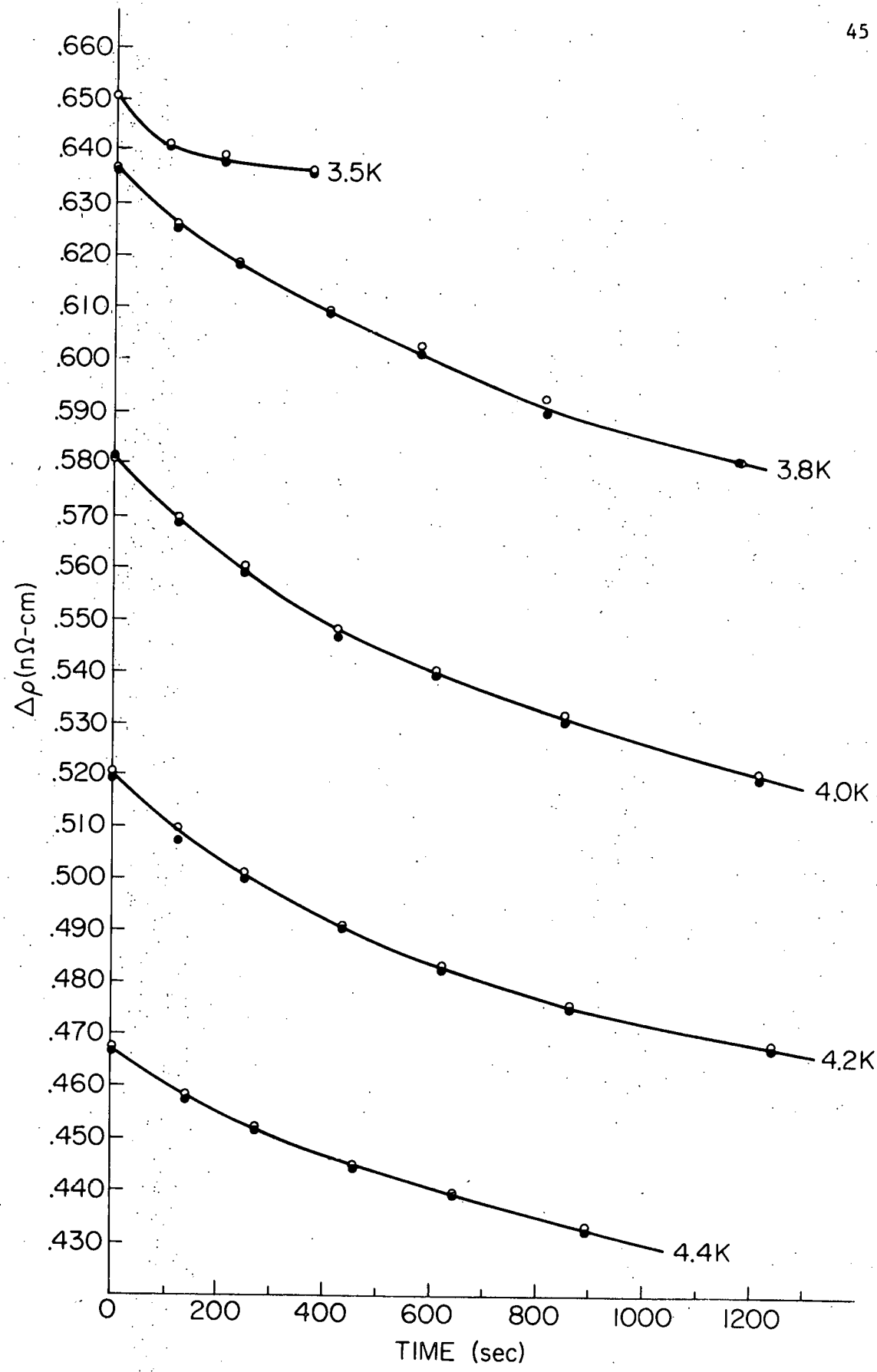
.660
.650
.640
.630
.620
.610
.600
.590
.580
.570
.560
.550
.540
.530
.520
.510
.500
.490
.480
.470
.460
.450
.440
.430
Δρ(nΩ-cm)
3.5K
3.8K
4.0K
4.2K
4.4K
0
200
400
600
800
1000
1200
TIME (sec)

the I_D substage. The final anneal at 4.4 K involves both the I_D and the I_E substages. The slope change analysis[13] used for this experiment is not valid for recovery involving more than one thermally activated processes.

The activation energies calculated using the slope change analysis from the data in Figure 13 are shown in Table 1.

Table 1

Temperatures (K)	E (eV)
3.5 - 3.8	0.0055
3.8 - 4.0	0.0098
4.0 - 4.2	0.0099
4.2 - 4.4	0.0127

The first and last values are not expected to represent the thermal activation energy. The activation energy for the I_D peak is 0.0099 $\pm$ 0.001 eV. The pre-exponential factor for this first order reaction is 2×10^{12} sec^{-1} to within a factor of 4.

If both the I_C and I_D recoveries are assumed to be first order processes with the same pre-exponential factors, the change in slope between the 3.5 K and the 3.8 K isothermals gives an activation energy for the I_C substage of 0.0087 eV $\pm$ 0.001 eV.

D. Defect Concentration Dependence of the I_E Substage

In the isochronal annealing experiment the I_E recovery shifted to lower temperatures for higher initial defect concentrations. To fit

the recovery spectra shown in Figure 12 the I_E recovery was assumed to have the same thermal activation energy as the I_D recovery. The monomolecular rate equation, Eq. (7), was solved for first and second order kinetics. The theoretical recovery for a given order of kinetics depends on the reaction rate constant and the initial defect concentration. The I_E recovery spectrum for an initial measured resistivity change of 1.03 nΩ-cm was fitted with second order kinetics as shown in Figure 14a to determine the recovery rate constant. The exact shape of the calculated I_E recovery peak is very dependent upon the selection of the annealing temperatures. Removal of the calculated second order I_E recovery from the experimentally determined recovery leaves the I_o peak centered at 4.05 K with a half width of 0.6 K. The fitted I_E rate constant was used to calculate the recovery expected for a second sample with an initial measured resistivity change of 0.554 nΩ-cm. The change in the defect concentration for each sample can be determined by assuming a constant damage production rate and knowing the fluences used produce to the damage in each sample. The expected second order I_E recovery is compared to the measured recovery in Figure 15a. The same procedure was used to fit these recoveries with third order kinetics as shown in Figure 14b and Figure 15b.

The I_E recovery seems to be better described by second order kinetics. It was not possible to achieve an accurate third order fit to the 1.03 nΩ-cm I_E recovery spectrum. Third order kinetics predicts too great a shift in the I_E recovery peak with defect concentration and too wide a recovery peak.

Figure 14. (a) Second and (b) third order fits to the I_E recovery spectrum of the sample of Figure 12 for an initial measured resistivity change of 1.03 nΩ-cm.

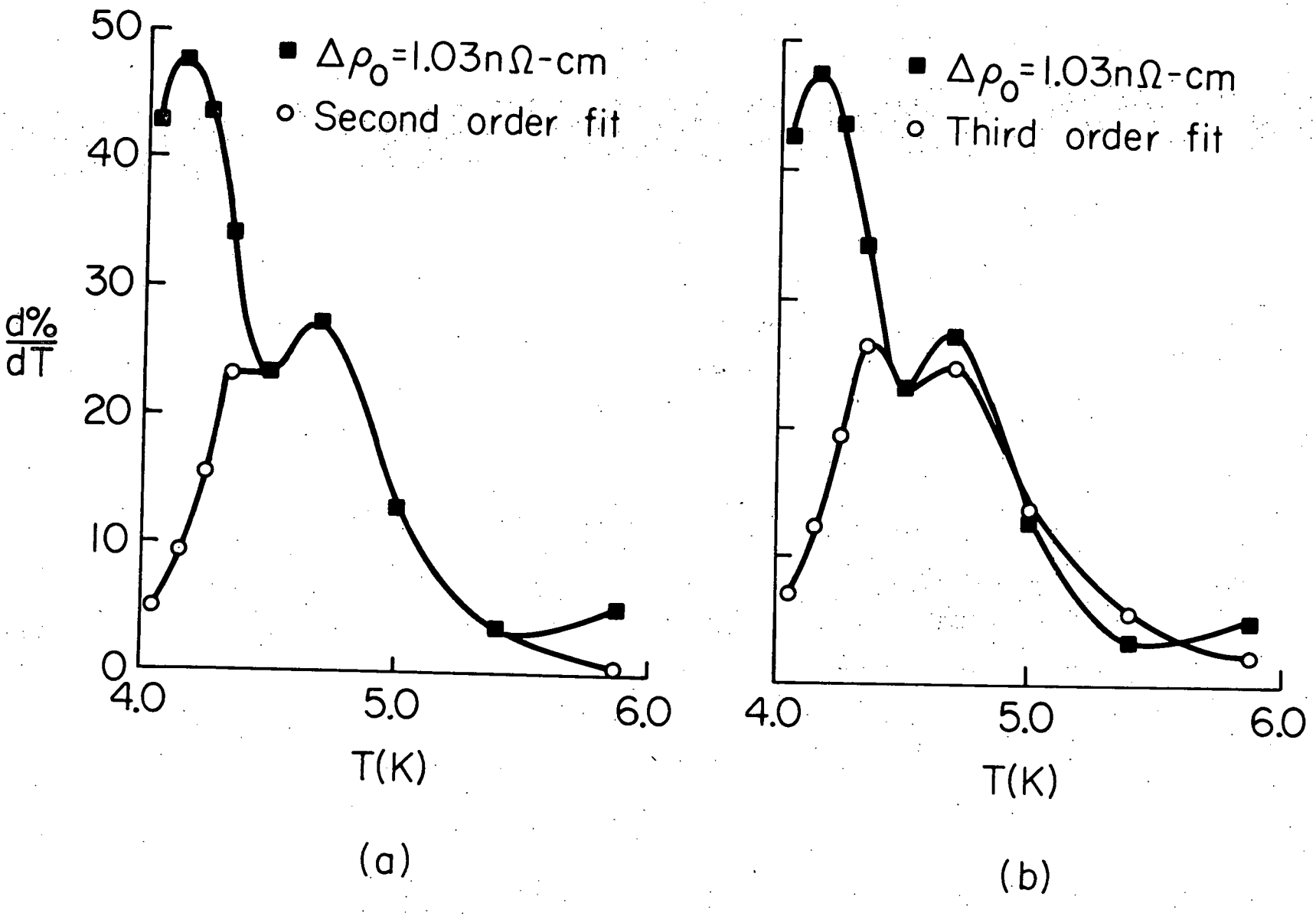
50
40
30
20
10
0
d%/dT
■ Δρ0=1.03nΩ-cm
○ Second order fit
4.0
5.0
6.0
T(K)
(a)
■ Δρ0=1.03nΩ-cm
○ Third order fit
4.0
5.0
6.0
T(K)
(b)

Figure 15. (a) Second and (b) third order fits to the I_E recovery spectrum of the second sample of Figure 12 calculated using the reaction rate constants determined in Figure 14.

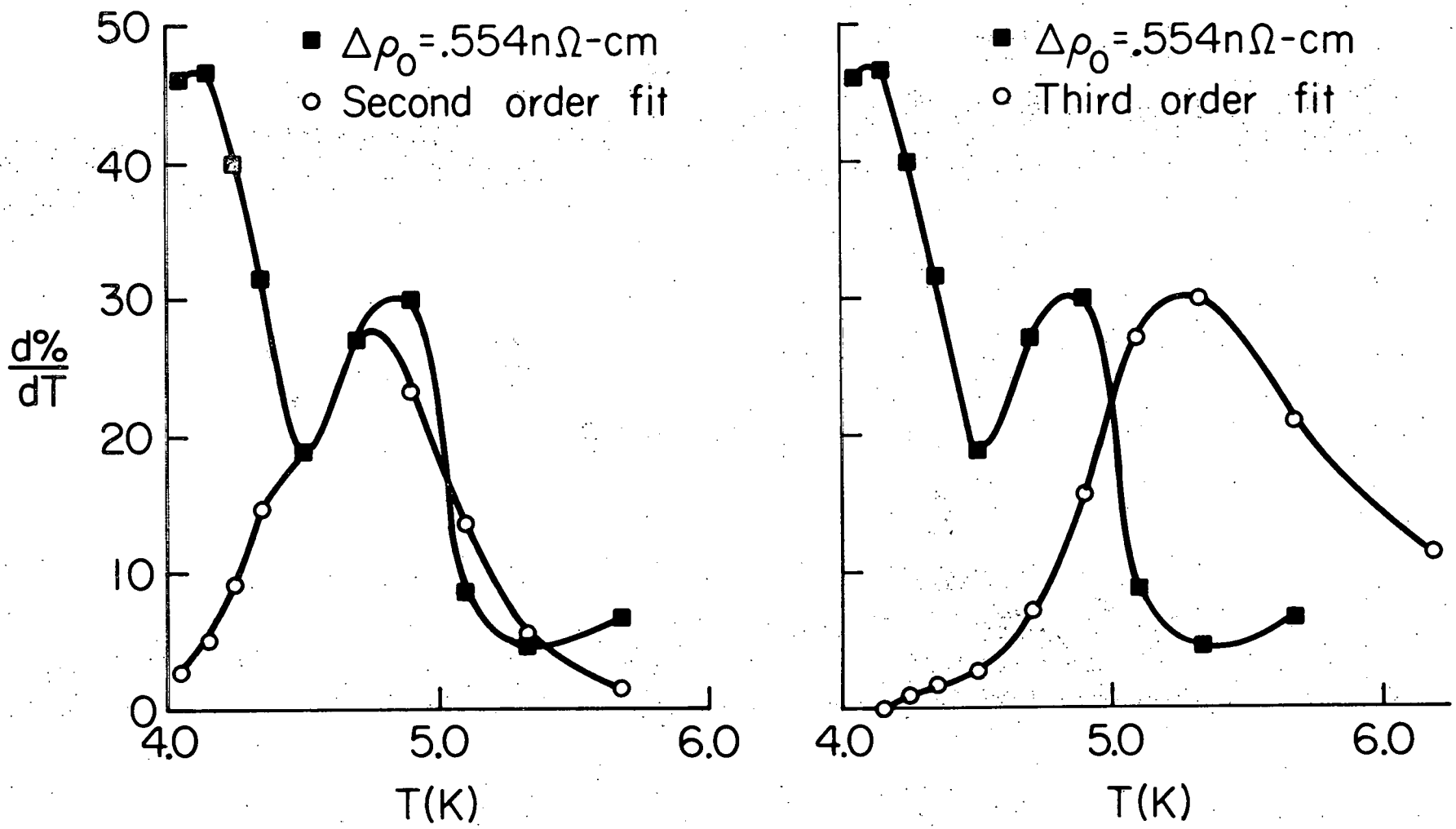
■ $\Delta\rho_0$=.554nΩ-cm
○ Second order fit
50
40
30
20
10
0
d%/dT
4.0
5.0
6.0
T(K)
(a)
■ $\Delta\rho_0$=.554nΩ-cm
○ Third order fit
4.0
5.0
6.0
T(K)
(b)

E. Activation Energy of the I_E Substage

During the isochronal anneal of the low dose (0.122 nΩ-cm) irradiation shown in Figure 11, following the anneal at 5.0 K for five minutes, an anneal was performed at 4.0 K for forty minutes. The 5.0 K anneal was at the end of the I_D substage and at the start of the I_E substage. The 4.0 K annealing temperature was 0.15 K lower than the temperature of the maximum rate of recovery for the I_D substage. This anneal removed 0.90 ± 0.15% of the total damage.

A first order process centered at 4.15 K with an activation energy of 0.010 eV should have been completed before the 5.0 K anneal. During the 4.0 K anneal, a second order process centered at 5.2 K with an activation energy of 0.010 eV should have recovered an additional 3% of the damage that recovers in the I_E stage. About 55% of the total damage remained after the 5.0 K anneal. If all this recovered in the I_E substage, about 1.6% would have recovered during the 4.0 K anneal. This over estimates the expected recovery because a large fraction of the remaining interstitials are trapped at impurities or other interstitials. Only 20% of the total damage recovered in the I_E substage. Thus one might expect 0.6% of the total damage to recover during the 4.0 K anneal. These rough estimates give upper and lower limits on the expected recovery. However, if the calculation is repeated with an activation energy of 0.011 eV, the recovery is expected to be between 0.04% and 0.09% of the total damage. Thus the I_E substage appears to have the same activation energy as the I_D substage to within 0.001 eV.

IV. SUMMARY OF THE EXPERIMENTAL RESULTS

The low temperature recovery of lead following an electron irradiation at 1.5 K shows the same features observed for all fcc metals except for gold. The low temperature recovery can be interpreted in terms of the split interstitial model originally proposed for copper.

The Stage I occurs below 5.5 K and has five substages. The lowest four substages obey first order annealing kinetics. The I_A substage is suppressed by subthreshold collision recovery events. The most predominant recovery begins in the I_D recovery which is centered at 4.15 ± 0.05 K. The activation energy for the I_D recovery is 0.010 eV ± 0.001 eV. The activation energy for the I_C substage has been inferred to be 0.0087 eV ± 0.001 eV with the assumption of the same pre-exponential factor as I_D. The I_E recovery shifts with defect concentration in lead as it does in copper. It obeys second order kinetics with an activation energy of 0.010 eV ± 0.001 eV.

The Stage II recovery begins at 5.8 K. This recovery extends in temperature up to Stage III[10,18] at about 160 K. Thus the recovery of the low temperature electron radiation damage of lead has all the features observed for copper.

APPENDIX A

SUPPLEMENTARY ISOCHRONAL RECOVERY DATA

Figure A. Isochronal recovery of four samples irradiated to measured resistivity changes of 0.378 nΩ-cm, 0.581 nΩ-cm, 0.762 nΩ-cm and 1.10 nΩ-cm respectively.

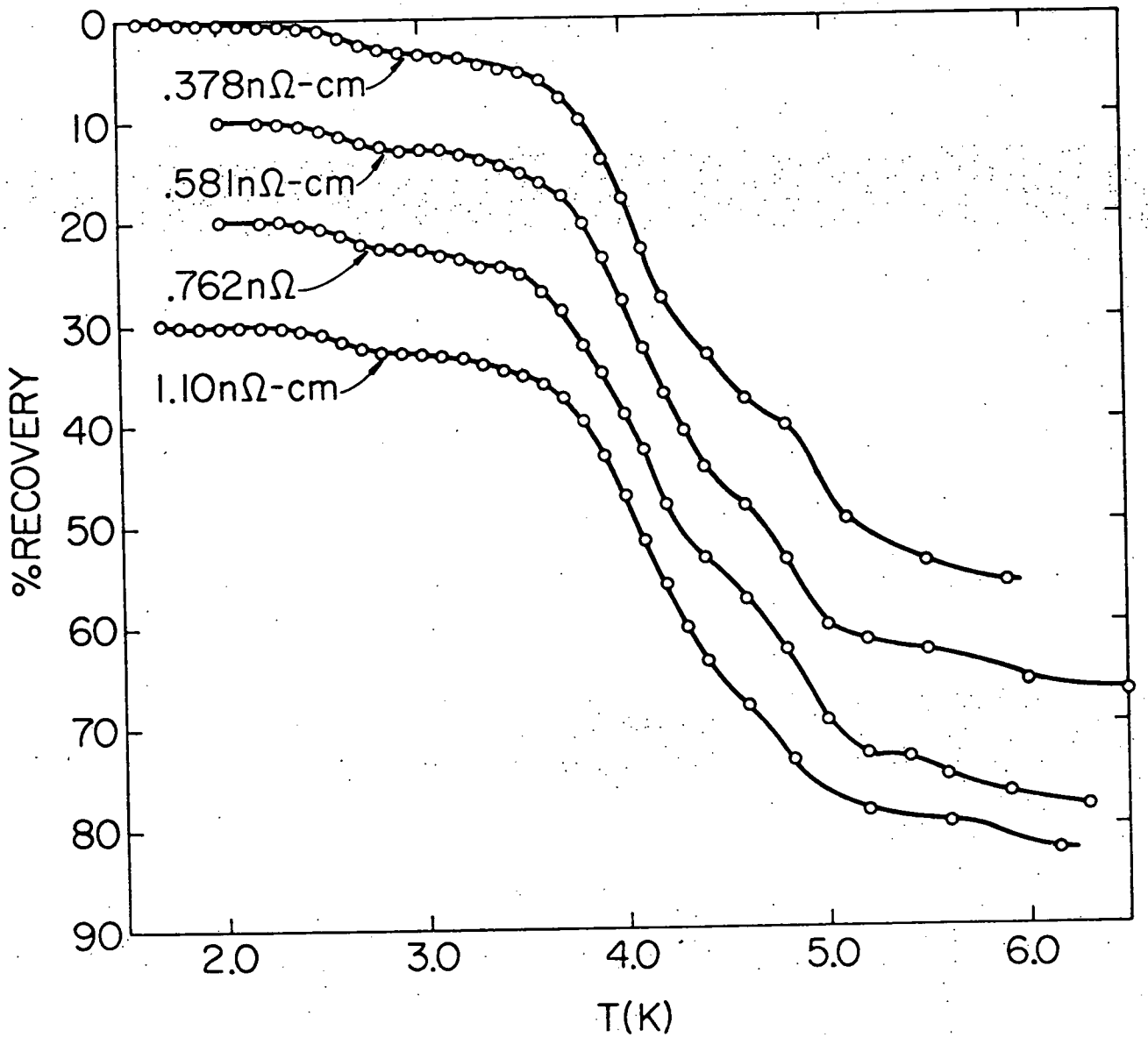
0
10
20
30
40
50
60
70
80
90
%RECOVERY
.378nΩ-cm
.581nΩ-cm
.762nΩ
1.10nΩ-cm
2.0
3.0
4.0
5.0
6.0
T(K)

APPENDIX B

FITTING PROCEDURE FOR THE I_E SUBSTAGE

For defect recovery described by the monomolecular rate equation, the time dependence of the resistivity is given by

$$\frac{d\rho}{dt} = - A \rho^{(n+1)} e^{-E/kT} \tag{B1}$$

where (n+1) is the order of the kinetics of the reaction and the resistivity has been assumed to be proportional to the defect concentration. After the first anneal to the temperature T_1 for a time t the remaining resistivity ρ_1 is given by

$$\left(\frac{1}{\rho_1}\right)^n = \left(\frac{1}{\rho_o}\right)^n + A\, t e^{-E/kT_1} \tag{B2}$$

where ρ_o was the initial resistivity and $n > 1$. After m anneals, all for a time t, the remaining resistivity is given by

$$\left(\frac{1}{\rho_m}\right)^n = \left(\frac{1}{\rho_{m-1}}\right)^n + A\, t e^{-E/kT_m} \tag{B3}$$

$$\left(\frac{1}{\rho_m}\right)^n = \left(\frac{1}{\rho_o}\right)^n + A\, t \sum_{i=1}^{m} e^{-E/kT_i} \tag{B4}$$

The % recovery after m anneals is given by

$$\frac{\rho_m}{\rho_o} = \left[1 + A \rho_o^n\, t \sum_{i=1}^{m} e^{-E/kT_i}\right]^{-1/m} \tag{B5}$$

This equation has been used to fit the I_E recovery for second (n = 2) and third (n = 3) order kinetics to determine the reaction rate constant A. Using A, the expected recovery for a different defect concentration may be calculated.

REFERENCE

1. W. Schilling and K. Sonnenburg, J. Phys. F 3, 322 (1973).

2. P. S. Gwozdz and J. S. Koehler, Phys. Rev. B 8, 3616 (1973).

3. R. C. Birtcher, Y. N. Lwin, and J. S. Koehler, Phys. Rev. Lett. 33, 899 (1974).

4. J. W. Corbett, Electron Radiation Damage, Supplement 7 of Seitz and Turnbull Solid State Physics series (Academic Press, New York, 1966), Chapter 6.

5. M. J. Berger and S. M. Seltzer, Tables of Energy Losses and Ranges of Electrons and Positrons (NASA Scientific and Technical Information Division, Washington, D.C., 1964).

6. H. Van Dijk, M. Durieux, J. R. Clement, and J. K. Logan, Physica 24, S129 (1958).

7. R. A. Scribner and E. D. Adams, Temperature, Its Measurement and Control in Science and Industry (Instrument Society of America, Pittsburgh, 1972), Vol. 4, Part 1, p. 773.

8. J. P. Franck and D. L. Martin, Can. J. Phys. 39, 1320 (1961); P. H. Boecherds, Rev. Sci. Instrum. 9, 138 (1969).

9. R. Guenther, H. Weinstock, and R. W. Schleicher, Cryogenic Technology 6, 13 (1970).

10. W. H. Keesom, B. F. Saris, and L. Meyer, Physica 7, 817 (1940).

11. Y. S. Touloukian, ed., Thermophysical Properties of Matter, Vol. 1 (IFI/Plenum, New York-Washington, 1970), p. 175.

12. B. N. Aleksandrov and I. G. D'Yakov, Soviet Phys. JETP 16, 603 (1963).

13. R. G. Chambers, Proc. Roy. Soc. (London) 202, 378 (1950).

14. Y. H. Kao, Phys. Rev. 138, A 1412 (1965).

15. H. Schroeder, Ph. D. Thesis, Rheinisch-Westfälischen Technischen Hochschule Aachen, 1974.

16. A. W. Overhauser, Phys. Rev. 90, 393 (1953).

17. G. Duesing, W. Sassin, W. Schilling, and H. Hemmerich, Cryst. Latt. Def. 1, 55 (1969).

18. Y. N. Lwin, E. A. Ryan, R. C. Birtcher, and J. S. Koehler, Bull. Am. Phys. Soc. 19, 256 (1974).

VITA

Robert Charles Birtcher was born on August 30, 1946 in Fort Wayne, Indiana. He received a B. S. degree in Physics from the University of Illinois in June 1968. He entered the Graduate College, University of Illinois, in September 1968 and received a M. S. degree in Physics in June 1970. He held teaching and research assistantships while at the University of Illinois. He is a co-author of five papers entitled "Temperature Variation of the Resistivity of Epitaxial Gold Films", J. Vac. Sci. Technol. 7, 339 (1970); "Valence Band Structure in Silver Fluoride", J. Phys. C 5, 562 (1972); "Production and Recovery of Pure Lead Using Electron Irradiation at 3 K, 5 K and 8 K", Bull. Am. Phys. Soc. 19, 256 (1974); "Isochronal Annealing of Pure Lead Electron Irradiated at 1.5 K", Phys. Rev. Lett. 33, 899 (1974); and, "Recovery of Pure Indium Following Electron Irradiation at 5 K", Bull. Am. Phys. Soc. (to be published).